Efficient polymer light-emitting diodes (PLEDs) based on chiral [Pt(C^N)(N^O)]-complexes with near-infrared (NIR) luminescence and circularly polarized (CP) light

COMMUNICATION

Efficientpolymer light-emitting diodes (PLEDs) based on chiral [Pt(C^N)(N^O)]-complexes with near-infrared (NIR) luminescence and circularly polarized (CP) light

Guorui Fu,[‡,a] Yani He,[‡,a] Wentao Li,[a] Baowen Wang,[a] Xingqiang Lü,[*a] Hongshan He[*b] and Wai-Yeung Wong[*c]

Based on molecular design of chiral NIR-emitters [Pt(iqbt)(S-L^n)] (1-4), the first example CP-NIR-PLEDs with both attractive NIR-emissive properties (λ_{em} = 732 nm; η_{EQE}^{Max} = 0.87-0.93%) and high dissymmetry g_{EL} factors up to 10^{-3} are reported.

Circularly polarized (CP) light-active materials,[1] due to the tracking of specific interactions with chiral environments, have recently attracted particular interest on chiral optoelectronics.[2] Especially independence on the direct generation of CP light, CP organic/polymer light-emitting diodes (OLEDs/PLEDs)[3] advantageous of achieving high contrast 3D images and true backlight, are significantly superior to routine OLEDs/PLEDs. To date, studies on small-molecule-[4] or polymer[5] with $^1\pi$-π*-transitioned fluorescence have been reported. When thermally-activated delayed fluorescence (TADF)[6] system, transition-metal complex[7] or organo-Ln^{3+} complex[8] are employed, their capability of harvesting both ^{1}S and ^{1}T excitons for vivid visible (λ_{em} = 400-700 nm) CP-OLEDs/PLEDs makes the resulting devices more appealing. In particularly, the CP devices that emit in the NIR (NIR = near-infrared; λ_{em} > 700 nm) offer numerous advantages for bioassay, information-security and night-version readable display.[9] However, the study in this direction is much scarce, which can be attributed to several challenges including unavoidable CP-active materials' aggregation and lack of NIR-active chiroptical luminogen.

As a matter of fact, Pt(II)-complex phosphors have achieved great success in the development[10] of efficient NIR-OLEDs/PLEDs. In this context, one elegant strategy toward that restrictive NIR regime for typical vacuum-deposited NIR-OLEDs is focused on the significant bathochromatic-shift of sublimed Pt(II)-complexes caused by unforeseen excimers' formation and strong Pt···Pt-

interacting-within intermolecular interactions. However, besides the contention[11] of aggregation-induced quenching or enhancement of emission (AIQ or AIE), the realization of their η_{EQE} up to the unit[12] or even the tenth[13] actually trades off the inevitable high-cost of device fabrication and aggregation-induced detrimental efficiency-roll-off. Convincingly, circumventing such problems for the compromise of cost-effectiveness and desirable device performance (high-efficiency while relatively weak efficiency-roll-off), solution-processable NIR-OLEDs/PLEDs[14] based on homogeneous doping of Pt(II)-complex just with the strong MLCT effect into an appropriate host with the deep HOMO-LUMO bandgap should be more considerable as an alternative. Whereas the development of highly emissive NIR-OLEDs/PLEDs without Pt(II)-chromophores' interactions remains a great challenge due to the "energy gap law"[15] limit. Nuzzo et al[16] used a chirally substituted polymer doped with achiral Pt(II)-complex as the emitting material and fabricated the device with emission around 550 nm. Fuchteret al[17] incorporated a chiral Pt(II)-complex into a conventional light-emitting polymer and the CP-electroluminescence was observed around 600 nm. Herein, in light of the deserved NIR (λ_{em} = 707 nm) emission[18] of [Pt(iqbt)(dpm)] (Scheme 1), we report the first example of CP-NIR-PLEDs by ingeniously introducing simplex chirality into the N^O-Schiff-base ancillary ligands S-HL^n (n = 1-4) for their chiral [Pt(iqbt)(S-L^n)]-heteroleptic complexes (1-4; also Scheme 1). Both CP-light activity and NIR electroluminescence (732 nm) were observed. This result demonstrated the potential application of chiral NIR-emitting Pt(II)-complexes in solution-processable CP-NIR-PLEDs.
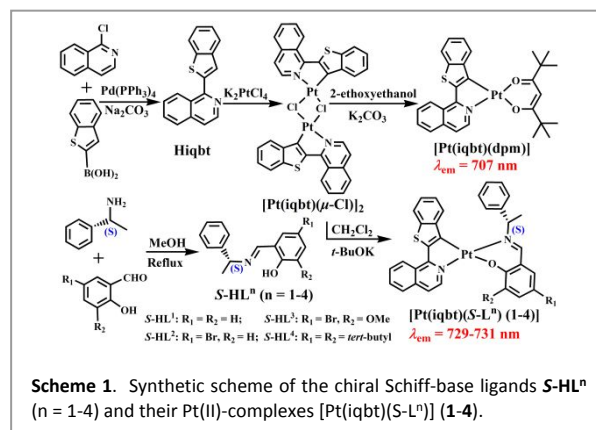
^{a}School of Chemical Engineering, Shaanxi Key Laboratory of Degradable Medical Material, Northwest University, Xi'an 710069, Shaanxi, China.
^{b}School of Chemistry, Eastern Illinois University, Charleston, IL 61920, USA
^{c}Department of Applied Biology and Chemical Technology, The Hong Kong Polytechnic University, Hung Hom, Hong Kong, P.R. China
†E-mail: lvxq@nwu.edu.cn; hhe@eiu.edu; wai-yeung.wong@polyu.edu.hk; Tex/Fax: +86-29-88302312
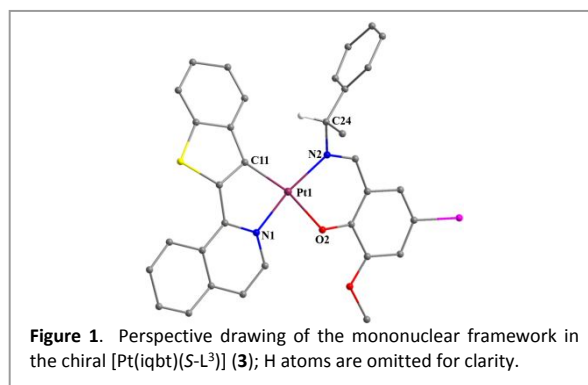Electronic Supplementary Information (ESI) available: [Starting materials and characterization; XRD; UV, PL]. See DOI: 10.1039/x0xx00000x
‡These authors contributed equally and should be considered co-first authors.

Scheme 1. Synthetic scheme of the chiral Schiff-base ligands S-HL^n (n = 1-4) and their Pt(II)-complexes [Pt(iqbt)(S-L^n)] (1-4).

Based on reaction (also Scheme 1) of K_2PtCl_4 with the C^N-cyclometalated ligand **Hiqbt** synthesized from the Suzuki coupling of cost-effective 2-Cl-isoquinoline[19] with benzo[*b*]thien-2-y boronic acid, the *µ*-chloro-bridged dimer intermediate **[Pt(iqbt)(*µ*-Cl)]₂** was obtained in 89%. As to the chiral Schiff-base-typed ligands *S*-**HLⁿ** (n = 1-4), they were prepared from the rational condensation[20] of *S*-(-)-1-phenylethylamine with one of the salicylaldehyde derivatives, respectively. Further through the treatment of **[Pt(iqbt)(*µ*-Cl)]₂** with each of the chiral ligands *S*-**HLⁿ** (n = 1-4) in the presence of *t*-BuOK, the targeted chiral Pt(II)-complexes [Pt(iqbt)(*S*-Lⁿ)] (**1-4**) soluble in common organic solvents, were afforded, respectively.

The chiral Schiff-base-typed ligands *S*-**HLⁿ** (n = 1-4) and their Pt(II)-complexes **1-4** were well-characterized by EA, FT-IR, ¹H NMR (Figures S1-2) and ESI-MS. All the Pt(II)-complexes exhibited relatively high thermal stabilities. TGA results (Figure S3) of the chiral Pt(II)-complexes **1-4** show that their high decomposition temperatures (T_d, corresponding to 5% weight loss; 230 °C for **1**,267 °C for **2**,239 °C for **3** or 214 °C for **4**) were observed. As to the more favourable thermal stability with the electron-drawing Br atom for **2** while an opposite trend with the electron-donating *tert*-butyl groups for **4**, it can be reasonably explained by the relatively shorter Pt-C (1.99421 Å), Pt-N (2.05599-2.06234 Å) and Pt-O (2.11856 Å) bond lengths (Table S1) for **2** than those (Pt-C (2.00438 Å), Pt-N (2.05585-2.06706 Å) and Pt-O (2.12124 Å)) for **4** from the following TD-DFT calculations. Molecular structure of [Pt(iqbt)(*S*-L³)] (**3**) was confirmed by X-ray single-crystal diffraction analysis. The complex crystallizes in the triclinic space group of *P*1, whereas the non-centrosymmetric nature originates from the (*S*-L³)⁻-induced chirality. As shown in Figure 1, one C11^N1-chelate (**iqbt**)⁻ ligand and one ancillary ligand (*S*-L³)⁻ with the N2^O2-chelate mode, coordinate to the central Pt²⁺ ion (Pt1) in a square planar geometry, leading to the formation of a typical asymmetric mononuclear framework.[18] Noticeably, different from the *co*-planar conformation of the cyclometalated (**iqbt**)⁻ ligand, the terminal phenyl ring of the chiral (*S*-L³)⁻ ligand is almost perpendicular to its N2^O2-chelate plane with a dihedral angle of 84.1(2)°, from which, the *S*-chiroptical character centered at the chiral -C*24-H atom for [Pt(iqbt)(*S*-L³)] (**3**) is well-retained. Interestingly, complementary intermolecular interactions (3.566(2) Å of π···π, 3.791(2) Å of π···Pt and 3.710(30) Å of C18-H18···π; Figure S4) while no valid Pt···Pt interactions, are observed between every adjacent two mononuclear units, giving rise to the 1D polymeric chain. The crystallographic data of this compound can be found in Tables S2-3.

Photophysical properties of the chiral Pt(II)-complexes **1-4** in solution or solid-state were explored at RT or 77 K (Table S4 and Figures 2-3 and S5-9. As shown in Figure 2, chiral Pt(II)-complexes **1-**
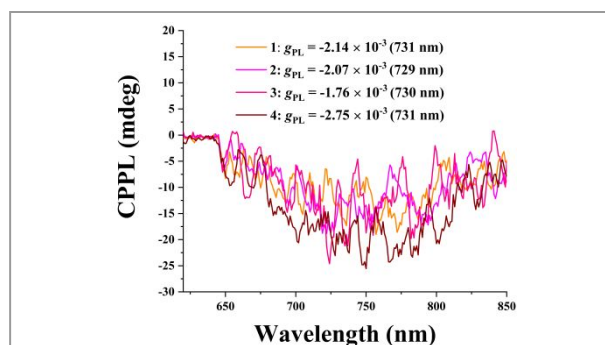

Figure 1. Perspective drawing of the mononuclear framework in the chiral [Pt(iqbt)(*S*-L³)] (**3**); H atoms are omitted for clarity.

spectra than those (λ_{ab} < 400 nm; Figure S5) of the **Hiqbt** and *S*-**HLⁿ** ligands: the high energy-state intense absorption in the 200-400 nm range assigned to the ligands-based ¹π-π* transitions, and the relatively weak absorptions (λ_{ab} > 430 nm) probably attributed to a mixed ¹,³LLCT/¹,³MLCT transitions. The substituents on the (*S*-Lⁿ)⁻ ligands have little effect on the absorption and CD spectra (Figure S6) of their Pt(II)-complexes. Importantly, contrasted to the ligand-relative visible emissions (Figure S7) for both the **Hiqbt** and *S*-**HLⁿ** ligands, all the chiral four Pt(II)-complexes **1-4** display the unique NIR-emissive emission spectra in solution at RT also as shown in Figure 2, featuring with a strong peak located at λ_{em} = 730 nm and a shoulder at 806 nm. Among the split two peaks (0-0 transitioned λ_{em} = 730 nm and 0-1 transitioned λ_{em} = 860 nm) relative to a different degree of vibrational coupling, the lower-energy emission peak is probably constituted by the high-frequency normal modes with larger Huang-Rhys factors.[21] Their phosphorescent properties show a structural profile: a short lifetime of 0.88 *µ*s for **1**, and a significantly longer 1.02 *µ*s **2** or 0.96 *µ*s for **3** should result from the Br-facilitated intersystem-crossing. The electron-donating effect of two -*tert*-butyl groups should contribute to the shortest one (0.85 *µ*s) for the (*S*-L⁴)⁻-involved **4**. It is worth noting that all the NIR-emissive efficiencies (Φ_{PL}) of the four chiral Pt(II)-complexes are also regulated from the (*S*-Lⁿ)⁻-involved electronic effects, and their attractive Φ_{PL} centered at 731 nm among reported NIR-emissive Pt(II)-complexes[10] just with the MLCT impaction, should be attributed to their large radiative rate constant (k_r = 10⁵ s⁻¹). The Br-incorporated chrial Pt²⁺-complex **2** gives rise to the best NIR-emissive Φ_{PL} of 21% due to the largest k_r (2.10×10⁵ s⁻¹) while the smallest k_{nr} (7.75×10⁵ s⁻¹). The effective radiative transition with the weak vibrational coupling for the four chrial Pt²⁺-complexes **1-4** can be further confirmed by their rigidochromic shifts (Figure S8) at 77 K, whereas the (*S*-Lⁿ)⁻-incorporation profits to effectively sidestep the intramolecular rotation/distortion for more chance to the T₁-
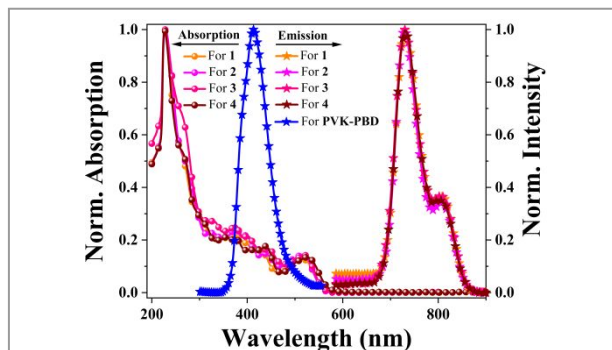
Figure 2. The normalized UV-visible absorption and emission spectra of the chiral Pt(II)-complexes **1-4** in degassed solution or PVK-PBD in solid-state at RT.

Figure 3. The CP light spectra of the the chiral Pt(II)-complexes **1-4** in degassed solution at RT.

4 in solution show the significantly broadened UV-visible absorption

preferred radiative decaying with longer phosphorescent lifetimes.

COMMUNICATION

As to the slight blue-shifts (λ_{em} = 725-727 nm) for **1-2** while red-shifts (λ_{em} = 741-751 nm) of **3-4** in solid-state (Figure S9) relative to that (λ_{em} = 732 nm) in solution at RT, it should probably be caused by strong intermolecular interactions (also Figure S4) as in the case of routine Pt^{2+}-complexes.

In their CD spectra (also Figure S6), besides the Cotton effects with two positive signals at 259-268 and 328-331 nm and an negative one at 286-313 nm like the free **S-HL^n** ligands, additional broad Cotton-effect bands came from the (**S-L^n**)$^-$-regulated exciton-coupling ^{1,3}LLCT/^{1,3}MLCT transitions with three negative signals and two positive signals within 355-600 nm. As to the emissive dissymmetry factor (g_{PL}; Figure 3) of the (**S-L^n**)$^-$-involved four chiral Pt(II)-complexes, it is at the degree of 10^{-3}, endowing a (**S-L^n**)$^-$-regulated size (-2.14×10^{-3} (731 nm) for **1**; -2.07×10^{-3} (729 nm) for **2**; -1.76×10^{-3} (730 nm) for **3** or -2.75×10^{-3} (731 nm) for **4**) at the corresponding NIR-emission peak probably due to the differential electron cloud shares[22] especially within the chiral (**S-L^4**)$^-$ portion (also Table S4 and Figure S10).

The theoretical studies provided further insights of the photophysical properties of these chiral complexes [Pt(iqbt)(**S-L^n**)] (**1-4**). The TD-DFT calculations (Table S5 and Figure S10) indicated that each of chiral Pt(II)-complexes **1-4** has the similar electron density distribution patterns to the LUMO+1 or LUMO, corresponding to the major contribution from the (**S-L^n**)$^-$ ligand (90.20-93.04%) or the (**iqbt**)$^-$ ligand (90.40-90.68%), respectively. The electron density of the HOMO is dominated by the ligands with the increased contribution from the (**iqbt**)$^-$ ligand (43.90%) than that from the (**S-L^1**)$^-$ ligand (38.36%) for **1**. This is different to the situation in **2-4** (47.81% for **2**, 59.87% for **3** or 60.48% for **4**) from the (**S-L^n**)$^-$ (n = 2-4) ligand. It was found that the introduction of 3-position MeO/*tert*-butyl and/or 5-position Br/*tert*-butyl groups for **2-4** gives a preferred contribution (53.47% for **2**, 62.32% for **3** or 63.88% for **4**) of the (**iqbt**)$^-$ ligand to their HOMO-1s. The Br substantially causes the destabilizations of both the HOMOs and LUMOs levels while an opposite stabilization from the MeO- or *tert*-butyl- group is observed. Hence, the relatively narrow HOMO-LUMO bandgaps (2.86 eV for **2**; 2.83 eV for **3** or 2.80 eV for **4**) relative to **1** (2.91 eV) were observed in **2-4**. Even though the calculated HOMO → LUMO transition (514 nm for **1**; 524 nm for **2**; 526 nm for **3** or 532 nm for **4**) came mainly (over 97%) from the S_0→ S_1 transition, the experimental lower-energy (λ_{ab} > 430 nm; 518-521 nm for **1-4**) absorptions should also include the LLCT/MLCT transitions. The NTO calculations (Table S6 and Figure S11) for S_0→ T_1 excitations indicated that about 80% hole orbital contribution from (**S-L^n**)$^-$ and 92% particle orbital contribution from the (**iqbt**)$^-$ ligand for each of the chiral Pt(II)-complexes **1-4**, constituted almost the entire (*ca.* 99%) Hole → Particle transition, suggesting that the ^{3}LLCT-dominated and the less ^{3}MLCT transitions, should be responsible for their NIR-emissive phosphorescence. This bandgap is quite similar to those determined electrochemically (Figure S12 and also Table S4).

It is of particular interest on the cost-effective and large-area flexible CP-NIR-PLEDs based on these chiral Pt(II)-complexes **1-4**. PVK-PBD was used as the appropriate host due to its good hole-electron transport, and the significant spectra overlap (also Figure 2) between the emission of PVK-PBD and the LLCT/MLCT absorption of the chiral Pt(II)-complexes **1-4** for effective Förster energy transfer[23] from PVK-PBD to the chiral Pt(II)-complex species. Since the LUMO (-2.95 ~ -2.86 eV) and HOMO (-5.66 ~ -5.61 eV) levels of the chiral Pt(II)-complexes **1-4** perfectly within those (-2.50 ~ -2.00 eV of LUMOs and -6.10 ~ -5.50. eV of HOMOs) of PVK and PBD, respectively, the injected holes from PEDOT:PSS and the injected
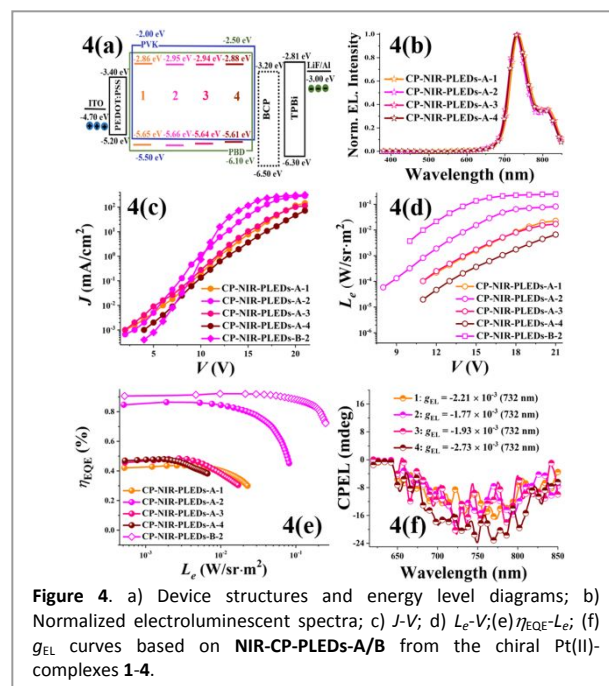
Figure 4. a) Device structures and energy level diagrams; b) Normalized electroluminescent spectra; c) *J-V*; d) L_e-*V*;(e)η_{EQE}-L_e; (f) g_{EL} curves based on **NIR-CP-PLEDs-A/B** from the chiral Pt(II)-complexes **1-4**.

electrons from TPBi pass through the PVK-PBD host to be trapped by the chiral Pt(II)-complex species, and subsequently, direct charge carrier trapping and recombination should take place. Through the solution-processable procedure with the same configuration shown in Figure 4(a), series of **CP-NIR-PLEDs-A/B** using the chiral Pt(II)-complexes **1-4** as the dopants with a stipulated doping of 8 wt% are fabricated. The difference lies in the fact that a hole blocking BCP-layer was added in the B series.

As shown in Table S7 and Figures 4(b)/S13, all the normalized electroluminescent NIR-emissive (λ_{em} = 732 nm) spectra for the series of **CP-NIR-PLEDs-A** are well resembled those of chiral Pt(II)-complexes **1-4** in solution at RT, which should arise from the low-concentration dispersion of the dopants **1-4** into the corresponding PVK-PBD host in the absence of those strong intermolecular interactions (also Figure S4). It also shows structure-featureless and an independence on the applied bias voltage. Within Figures 4(c-e) for the *J-V*, L_e-*V* and η_{EQE}-L_e correlations for **CP-NIR-PLEDs-A** with different chiral Pt(II)-complexes **1-4**, differently from the monotonous increasing of both the *J* and L_e values with the increase of the applied bias voltage, all the η_{EQE} increase first and insistently decrease throughout the corresponding illuminating regime. The highest device efficiency is observed for the **CP-NIR-PLED-A-2**, giving the η_{EQE}^{Max} of 0.87% with L_e = 0.002 W/sr·m^2 at *J* = 6.02 mA/cm^2 after 10.5 V of the V_{on} (the voltage of L_e = 5×10^{-4} W/sr·m^2). In comparison, both the η_{EQE}^{Max} and L_e^{Max} (0.44-0.49% and 0.007-0.023 W/sr·m^2) of all the other **CP-NIR-PLEDs-A** based on chiral Pt(II)-complexes **1** and **3-4** are relatively lower than those (0.87% and 0.081 W/sr·m^2) of the **CP-NIR-PLED-A-2**, which is consistent with the measured order of their Φ_{PL} results afforded by (**S-L^n**)$^-$-involved electronic effect for their chiral Pt(II)-complexes (**1-4**) in solution (also Table S4). Nonetheless, the longest T_1-decayed phosphorescent lifetime for the (**S-L^2**)$^-$-induced **2** with the 5-position electron-drawing -Br effect, renders its **CP-NIR-PLED-A-2** a significant efficiency-roll-off (48%) as compared to those (20-37%) of the other three devices. For optimization, the **CP-NIR-PLED-B-2** (also Figure 4(a)) with an additional hole-blocking BCP layer was fabricated. Delightfully, contributing from more excitons confined within the broadening recombination zone,[24] the distinctively

improved electroluminescent NIR-emissive property (also Figures 4(b-e)) is approached. First, besides the illuminating voltage down to 6.0 V, the L_e^{Max} is almost three times higher than that of the **CP-NIR-PLED-A-2**. Moreover, the reformed carrier balance within the **CP-NIR-PLED-B-2** also endows an attractive η_{EQE}^{Max} up to 0.93% among previous Pt(II)-complex-based NIR-PLEDs.[10,14] Interestingly enough, its efficiency-roll-off (23%) is also relieved. Worthy of notice, as shown in Figure 4(f), the dissymmetry factors (g_{EL}, also Table S7) of all the **CP-NIR-PLEDs** are also ruled by the (**S-Lⁿ**)⁻-relativity also within the 10^{-3} order as the reported Pt(II)-complex-based visible CP-OLEDs.[7]

In conclusion, through the involvement of (**S-Lⁿ**)⁻-N^O ancillary ligands with different electronic effects, series of chiral [Pt(iqbt)(**S-Lⁿ**)] complexes (**1-4**) with NIR-emissive (λ_{em} = 729-731 nm) and CPL-active properties were obtained. Moreover, based on their doping into the PVK-PBD host, the **CP-NIR-PLEDs** with the much attractive device performance (λ_{em} = 732 nm; η_{EQE}^{Max} up to 0.87-0.93%) and the high g_{EL} up to 10^{-3}, were first reported. This result suggests that the (**S-Lⁿ**)⁻-involved chiral [Pt(iqbt)(**S-Lⁿ**)]-complexes are promising candidates for future **CP-NIR-PLEDs**.

Notes and references

1. E. M. Sánchez-Carnerero, A. R. Agarrabeitia, F. Moreno, B. L. Maroto, G. Muller, M. J. Ortiz, S. de la Moya, *Chem. Eur. J.* 2015, **21**, 13488-13500.
2. Y. J. Zhang, T. Oka, R. Suzuki, J. T. Ye, *Science* 2014, **344**, 725-728.
3. J. M. Han, S. Guo, H. Lu, S. J. Liu, Q. Zhao, W. Huang, W. *Adv. Opt. Mater.* 2018, **6**, 1800538.
4. (a) M. Shimada, Y. Yamanoi, T. Ohto, S. T. Pham, R. Yamada, H. Tada, K. Omoto, S. Tashiro, M. Shionoya, M. Hattori, *J. Am. Chem. Soc.* 2017, **139**, 11214-11221; (b) H. Sakai, S. Shinto, J. Kumar, Y. Araki, T. Sakanoue, T. Takenobu, T. Wada, T. Kawai, T. Hasobe, *J. Phys. Chem. C* **2015**, *119*, 13937-13947.
5. (a) D. M. Lee, J. W. Song, Y. J. Lee, C. J. Yu, J. H. Kim, J. H. *Adv. Mater.* 2017, **29**, 1700907; (b) Y. Yang, R. Correa da Costa, D. M. Smilgies, A. J. Campbell, M. J. Fuchter, *Adv. Mater.* 2013, **25**, 2624-2628.
6. (a) M. Li, S. H. Li, D. D. Zhang, M. H. Cai, L. Duan, M. K. Fung, C. F. Chen, *Angew. Chem. In. Ed.* 2018, **57**, 2889-2893; (b) S. Feuillastre, M. Pauton, L. H. Gao, A. Desmarchelier, A. J. Riives, D. Prim, D. Tondelier, B. Gffroy, G. Muller, G. Clavier, *J. Am. Chem. Soc.* 2016, **138**, 3990-3993.
7. M. Ibrahim-Ouali, F. Dumur, *Molecules* 2019, **24**, 1412.
8. (a) F. Zinna, M. Pasini, F. Galeotti, C. Botta, L. Di Bari, U. Giovanella, *Adv. Funct. Mater.* 2017, **27**, 201603719; (b) F. Zinna, U. Giovanella, L. Di Bari, *Adv. Mater.* 2015, **27**, 1791-1795.
9. (a) Z. Guo, S. Park, J. Yoon, I. Shin, *Coord. Chem. Rev.* 2014, **43**, 16-29; (b) H. F. Xiang, J. H. Cheng, X. F. Ma, X. G. Zhu, J. J. Jason, *Chem. Soc. Rev.* 2013, **42**, 6128-6185.
10. (a) Y. M. Zhang, Y. F. Wang, J. Song, J. L. Qu, B. H. Li, W. G. Zhu, W.-Y Wong, *Adv. Opt. Mater.* 2018, **6**, 1800466; (b) C.-L. Ho, H. Li, W.-Y. Wong, *J. Organomet. Chem.* 2014, **751**, 261-285.
11. (a) K. Kenda, S. Kazuki, *Angew. Chem. Int. Ed.* 2019, **58**, 8632-8639; (b) M. Ju, Y. Hong, W. Y. Jacky, A. J. Qin, Y. H. Tang, B. Z. Tang, *Adv. Mater.* 2014, **26**, 5429-5479.
12. (a) F. Nisic, A. Colombo, C. Dragonetti, D. Roberto, A. Valore, J. M. Malicka, M. Cocchi, G. R. Freeman, J. A. G. Williams, *J. Mater. Chem. C*, 2014, **2**, 1791-1800; (b) E. Rossi, A. Colombo, C. Dragonetti, D. Roberto, F. Demartin, M. Cocchi, P. Brulatti, V. Fattori, J. A. G. Williams, *Chem. Commun.* 2012, **48**, 3182-3184.
13. (a) X. L. Yang, H. R. Guo, X. B. Xu, Y. H. Sun, G. J. Zhou, W. Ma, Z. X. Wu, *Adv. Sci.* 2019, **6**, 1801930; (b) K. Tuong Ly, R.-W. Chen-Chen, H.-W. Lin, Y.-J. Shiau, S.-H. Liu, P.-T. Chou, C.-S. Tsao, Y.-C. Huang, Y. Chi, *Nat. Photonics* 2017, **11**, 63-68;
14. (a) Z. R. Hao, F. Y. Meng, P. Wang, Y. F. Wang, H. Tan, Y. Pei, S. J. Su, Y. Liu, *Dalton Trans.* 2017, **46**, 16257-16268; (b) Y. M. Zhang, Z. Yin, F. Y. Meng, J. T. Yu, C. F. You, S. Y. Yang, H. Tan, W. G. Zhu, S. J. Su, *Organ. Electron.* 2017, **50**, 317-324; (c) N. Su, F. Y. Meng, P. Wang, X. Liu, M. B. Zhu, W. G. Zhu, S. J. Su, J. T. Yu, *Dyes and Pigm.* 2017, **138**, 162-168; (d) W. J. Xiong, F. Y. Meng, H. Tan, Y. F. Wang, P. Wang, Y. M. Zhang, Q. Tao, S. J. Su, W. G. Zhu, *J. Mater. Chem. C* 2016, **4**, 6007-6015; (e) K. R. Graham, X. Y. Yang, J. R. Sommer, A. H. Shelton, K. S. Schanze, J. G. Xue, J. R. Reynolds, *Chem. Mater.* 2011, **23**, 5305-5312; (f) J. R. Sommer, R. T. Farley, K. R. Graham, X. Y. Yang, J. R. Reynolds, J. G. Xue, K. S. Schanze, *ACS Appl. Mater. & Interfaces* 2009, **1**, 274-278.
15. Z. Andrea, M. Alessandro, C. Franco, *Adv. Funct. Mater.* 2019, **29**, 1807623.
16. D. Di Nuzzo, C. Kulkarni, B. D. Zhao, E. Smolinsky, F. Tassinari, S. C. J. Meskers, R. Naaman, E. W. Meijer, R. H. Eriend, *ACS Nano* 2017, **11**, 12713-12722.
17. Y. Yang, R. Correa da Costa, D. Smilgies, A. J. Campbell, M. J. Fuchter, *Adv. Mater.* 2013, **25**, 2624-2628.
18. M. Penconi, M. Cazzaniga, S. Kesarkar, P. R. Mussini, D. Ceresoli, A. Bossi, *Photochem. Photobio. Sci.* 2017, **16**, 1220-1229.
19. (a) J. Zhou, G. R. Fu, Y. N. He, L. N. Ma, W. T. Li, W. X. Feng, X. Q. Lü, *J. Lumin.* 2019, **209**, 427-434; (b) G. R. Fu, H. Zheng, Y. N. He, W. T. Li, X. Q. Lü, H. S. He, *J. Mater. Chem. C* 2018, **6**, 10589-10596.
20. A. C. Chamayou, S. Ludeke, V. Brecht, T. B. Freedman, L. A. Nafie, C. Janiak, C. *Inorg. Chem.* 2011, **50**, 11363-11374.
21. W. L. Cai, A. C. Zhao, K. Ren, R. X. He, M. Li, W. Shen, *J. Phys. Chem. C* 2019, **123**, 17968-17975.
22. Z. P. Yan, K. Liao, H. B. Han, J. Su, Y. X. Zheng, J. L. Zuo, *Chem. Commun.* 2019, **55**, 8215-8218.
23. F. N. Castellano, *Acc. Chem. Res.* 2015, **48**, 828-839.
24. T. Mori, Y. Masumoto, T. Itoh, *J. Photopolym. Sci. Tech.* 2008, **21**, 173-180.

Table of content only

Efficientpolymer light-emitting diodes (PLEDs) based on chiral [Pt(C^N)(N^O)]-complexes with near-infrared (NIR) luminescence and circularly polarized (CP) light

Guorui Fu, Yani He, Wentao Li, Baowen Wang, Xingqiang Lü, Hongshan He, and Wai-Yeung Wong

Using chiral NIR-emitters [Pt(iqbt)(S-L^n)] (**1-4**) as the dopants, their CP-NIR-PLEDs with λ_{em} = 732 nm, η_{EQE}^{Max} = 0.87-0.93% and g_{EL} up to 10^{-3} are realized.